scientific reports

Check for updates

OPEN

Gut microbiota and metabolic profile changes unveil the deterioration of alveolar bone inflammatory resorption with aging induced by D-galactose

Fangzhou Liu[1,5], Yanzi Yao[1,2,5], Yue Huang[1], Liangliang Luo[3], Qian Wang[1,4], Bin Chen[1,4] & Huan Hu[1,4]✉

The global aging population has led to a rise in age-related health issues, such as malnutrition, metabolic disorders, and even immune decline. Among these concerns, periodontitis holds particular significance for the well-being of the elderly. This study aimed to investigate the impact of aging on inflammatory resorption of alveolar bone in mice with periodontitis, with a specific focus on alterations in the intestinal microenvironment. To achieve this, we established a D-galactose (D-gal)-induced aging mouse model with periodontitis and employed histopathological staining, oxidative stress, and inflammatory factors analyses to assess the severity of periodontitis and the health status. Additionally, the 16S rRNA sequencing and untargeted metabolomics analysis were employed to investigate alterations in the intestinal microbiota and metabolites. Our results showed that D-gal-induced aging mice with periodontitis experienced more pronounced alveolar bone inflammatory resorption and disruptions in the gut barrier, accompanied by an overall decline in physical condition. The microbial composition and structure of aged mice also underwent significant modifications, with a decreased Firmicutes/Bacteroidetes (F/B) ratio. Furthermore, metabolomics analysis demonstrated that D-gal-induced aging primarily influenced lipids and lipid-like molecules metabolism, and enrichment observed in the rheumatoid arthritis and histidine metabolism pathways. These findings provide further evidence that the aging process exacerbates age-related alveolar bone loss (ABL) through disturbances in intestinal homeostasis.

Keywords Periodontitis, Aging, Alveolar bone inflammatory resorption, Intestinal flora, Fecal metabolomics

Population aging is an irreversible global trend, with average life expectancy having doubled in most developed countries over the past 200 years. This demographic shift poses novel challenges for safeguarding the oral health and well-being of older individuals[1]. Periodontitis, characterized by inflammation and degradation of periodontal tissues, is a chronic inflammatory condition that is widely prevalent and a leading cause of tooth loss in adults. Epidemiological studies have identified aging is a primary risk factor for both the prevalence and development of periodontitis[2–4]. Recent survey found that the prevalence of periodontitis among adults aged 65 and older in the United States ranges from 62.1 to 74.2%, with an average prevalence of 66.2%[5]. Beyond its directly impairing chewing function, periodontal disease triggers persistent immune and inflammatory responses, which have far-reaching health implications. Notably, the progression of periodontitis can exacerbate a range of systemic diseases commonly seen in the elderly, such as cardiovascular disease, diabetes, rheumatoid arthritis, cancer, lung disease, and cognitive impairment, leading to more severe health outcomes[6]. Therefore, addressing periodontal disease is crucial to improving and maintaining overall health in the aging population.

[1]School of Stomatology, Zunyi Medical University, Zunyi, China. [2]Department of Stomatology, Luoyang Maternal and Child Health Hospital, Luoyang, China. [3]School of Preclinical Medicine, Zunyi Medical University, Zunyi, China. [4]Microbial Resources and Drug Development Key Laboratory of Guizhou Tertiary Institution, Zunyi Medical University, Zunyi, China. [5]These authors contributed equally: Fangzhou Liu and Yanzi Yao. ✉email: huhuan1990@163.com

Aging leads to a decline in both innate and adaptive immune system functions, a process known as "immune senescence". One key mechanism involves senescence-associated secretory phenotype (SASP) exosomes, which stimulate dendritic cells (DCs) and T cells, leading to the elimination of antigen presentation. This deterioration in immune function increases susceptibility to infections, tumors, and inflammatory diseases, including periodontitis[7]. Immune senescence-associated cells contribute to aging and inflammatory response in periodontal tissues by releasing extracellular exosomes, ultimately resulting in alveolar bone loss (ABL)[8,9]. Additionally, senescent $CD4^+$ T lymphocytes downregulate CD28 expression, while $CD4^+CD28^-$ T lymphocytes promote the secretion of tumor necrosis factor alpha (TNF-α), interleukin-17A (IL-17A), and receptor-activator of nuclear factor-κB ligand (RANKL), all of which are linked to pathological bone loss. Senescent Th17 and Treg lymphocytes may also disrupt the balance between Th17 and Treg cells, impede osteoblast differentiation, promote osteoclast formation, and accelerate ABL[10,11].

To investigate the effects of aging on periodontitis, researchers often utilize animal models that simulate the physiological changes associated with aging. These models are typically categorized into natural aging models and accelerated aging models, depending on the presence of external intervention. Natural aging models are time-consuming and costly, with limited control over variables and low repeatability, complicating the study of specific aging mechanisms. In contrast, accelerated aging models use external interventions to induce aging more rapidly and with greater control[12]. One common method for accelerating senescence is D-galactose (D-gal)-induced aging. This reducing sugar is naturally present in the human body and commonly found in daily foods[13]. When administered at high levels, D-gal is catalyzed by galactose oxidase to form aldoses and hydroperoxides, which leads to the generation of reactive oxygen species (ROS). The accumulation of ROS results in oxidative stress, which in turn triggers inflammation, mitochondrial dysfunction, apoptosis, and accelerates aging[14]. Excessive ROS causes an imbalance in oxidation and activates proinflammatory mechanisms, primarily through lipid peroxidation. This heightened oxidative stress damages periodontal connective tissue, contributing to the destruction of periodontal attachment and exacerbating periodontitis[15].

In addition to its direct effects on periodontal tissues, aging also affects the intestinal barrier, which in turn influences the gut microbiota and its metabolic products. Aging-related dysfunction of the intestinal barrier is closely linked to internal metabolic disorders. Specially, aging diminishes the stability of intestinal-specific actin ACT-5, and the activity of intestinal alkaline phosphatase (IAP), leading to disruption of the intestinal barrier and functional abnormalities[16,17]. This disruption often coincides with alterations in the composition of the gut microbiota. Moreover, the intestinal microbiota can impact alveolar bone homeostasis through its effects on intestinal barrier integrity, intestinal immune response, and systemic endocrine metabolism[18]. To study host-microbe interactions, 16S rRNA sequencing is extensively employed due to its high efficiency, accuracy, and ability to provide culture-independent, rapidly updated data on the composition and structure of gut microbiota[19,20]. Additionally, untargeted fecal metabolomics serves as a valuable complement to microbiome studies by comprehensively and systematically detecting changes in small molecular metabolites within the host[21].

This study aims to provide a comprehensive analysis of the physiological, biochemical, and intestinal microenvironmental mechanisms through which aging impacts alveolar bone resorption. By employing fundamental experiments alongside advanced sequencing analysis, we will explore the cumulative effects of D-gal-induced aging on these interconnected physical processes.

Results

Aging worsens periodontal condition

The periodontitis models constructed by ligation were successfully established. Histological analyses revealed that among the four groups, the D + Lig group exhibited the most pronounced reticular hyperplasia in the sulcular epithelium of the periodontium, accompanied by conspicuous infiltration of inflammatory cells. Additionally, the junctional epithelium showed apical migration, proliferation, and elongation, resulting in the formation of deep periodontal pockets. The collagen fibers beneath the junctional epithelium displayed edema, degeneration, and subsequent loss (Fig. 1A). Furthermore, there was a significant decline in the height of the alveolar ridge (Fig. 1B, $p<0.05$), with an increased number of osteoclasts observed (Fig. 1C, $p<0.05$). Microscopically, these osteoclasts exhibited positive red cytoplasm and blue multinucleated nuclei, and augmented osteoclasts frequently indicated active resorption of alveolar bone. These histological changes observed in both macroscopic and microscopic periodontal tissues suggest that the D-gal-induced aging process exacerbates the deterioration of periodontal condition.

Aging influences the general state of periodontitis mice

Next, we assessed the influence of aging on the systemic state of organisms from three perspectives: systemic inflammation, oxidative stress, and immune decline. Compared to their previous robust mental state and appearance, aged mice exhibited a bleak and yellowish appearance with thinning of fur after 10 weeks of D-gal injection. They also showed signs of lethargy, frequently slouching in the corner of the cage or hiding under the bedding. There were no initial differences in body weight among the groups before modeling. Although all groups experienced weight gain after 10 weeks, the sham + Ph group demonstrated a faster average weight increase compared to other groups. Conversely, the D + Lig group exhibited the lowest average weight gain. Furthermore, regardless of age (young or old), periodontitis model mice had significantly lower body weights than periodontally healthy mice (Fig. 2A, $p<0.05$).

To assess the impact of D-gal-induced aging on systemic inflammatory response, we measured inflammatory cytokines in the serum. Compared to the sham + Lig and D + Ph groups, the D + Lig mice showed enhanced accumulation of TNF-α and interleukin-6 (IL-6) (Fig. 2B), indicating a more pronounced inflammatory state. Furthermore, we measured the state of oxidative stress by evaluating changes in serum markers. The modeling

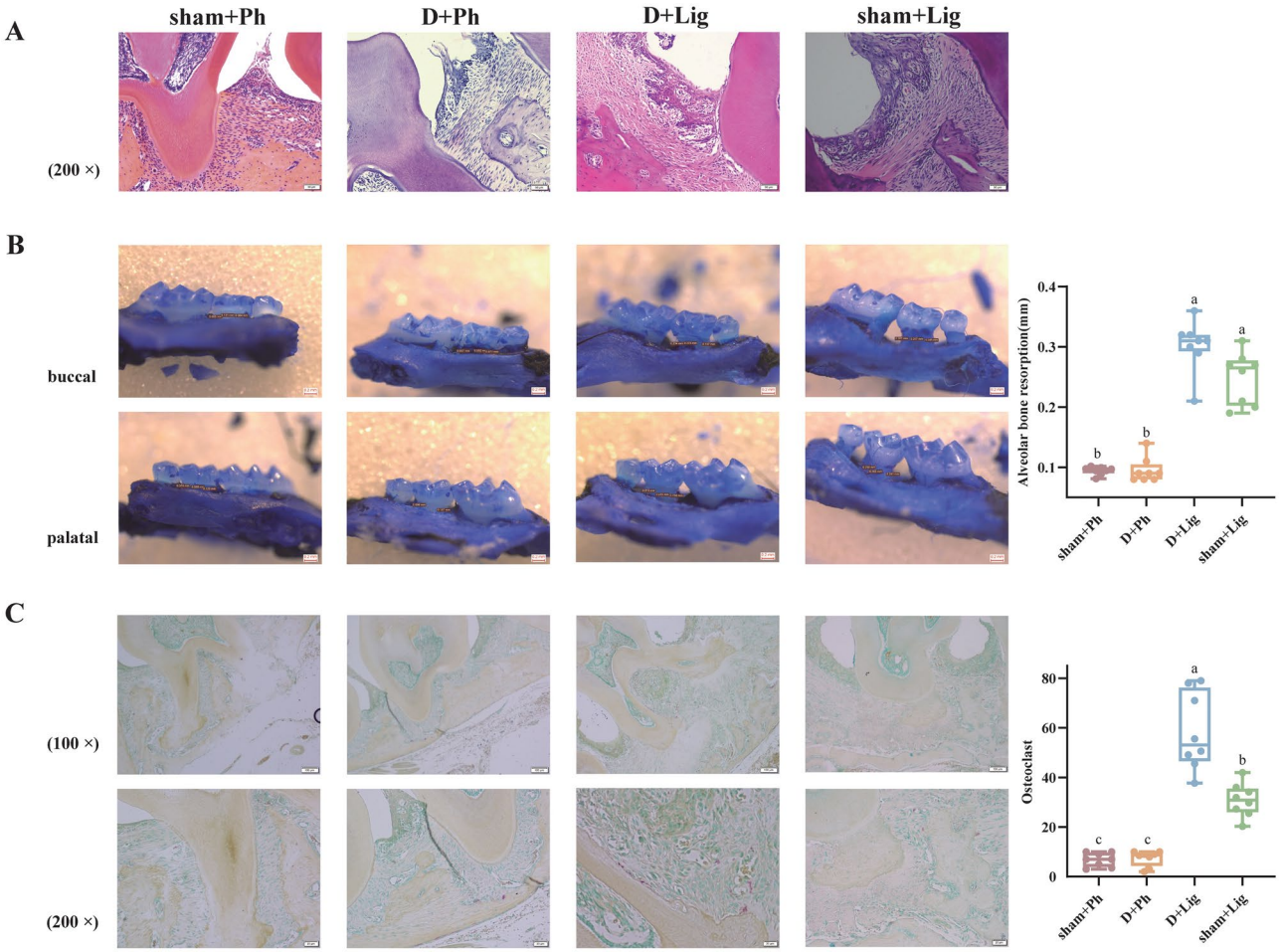

Fig. 1. D-galactose (D-gal)-induced aging aggravates alveolar bone inflammatory resorption (n = 8/group). (**A**) Representative images of Hematoxylin–eosin (HE) Staining in the periodontal tissues captured under a 200 × light microscope, (**B**) Representative images of Methylene blue staining of alveolar bone and average alveolar bone loss (ABL) value for the second molar, (**C**) Representative images of tartrate-resistant acid phosphatase (TRAP) Staining of positive multinucleated osteoclasts in the periodontal tissues captured under a 100 × and 200 × light microscope and the average quantity of osteoclasts surround the second molar. The upper and lower limits of each box in the boxplot show the upper quartile (75%) and lower quartile (25%) of each data set, the line in the middle of the box reflects the median values of each data set, and the lines above and below the box represent the maximum and minimum values. Statistical significance is denoted by differing letters on the top of the boxplot ($p < 0.05$). ABL, alveolar bone loss; D-gal, D-galactose; HE, Hematoxylin–eosin; TRAP, tartrate-resistant acid phosphatase.

procedure resulted in reduced superoxide dismutase (SOD) levels and elevated malonaldehyde (MDA) expression compared to the sham + Ph group, with the most notable effect observed in the D + Lig group (Fig. 2C, $p<0.05$). Lastly, the immunity organ indices were detected to evaluate discrepancies in immune status. We observed a reduced spleen index and thymus index in the D + Lig group when compared to sham + Lig group (Fig. 2D, $p<0.05$).

Moreover, we examined the heart, liver, and ileum in both groups to assess the impact of D-gal-induced aging on major organs. Histopathological results indicated that hepatocytes in the younger groups were closely arranged with large, round nuclei within the liver tissue. However, in the D + Ph and D + Lig groups, hepatocytes surrounding the central vein exhibited disorganization, with enlarged nuclei, loose cytoplasm, dark nuclear cytoplasm, and vacuole-like cells (Fig. 3A). The myocardial fibers in the sham + Ph and sham + Lig groups appeared elongated with branching connections forming a network structure, while cardiomyocytes displayed hypertrophy with widened gaps and disorganization, accompanied by increased cardiac muscle fiber connective tissue showing aging characteristics in the older groups (Fig. 3B). Additionally, occludin and zonula occludens-1 (ZO-1) proteins were primarily expressed in epithelial cells of the ileal mucosa where positive signals appeared as brown-yellow staining. In contrast to uniform continuous distribution at the edge of ileal epithelial cells seen in the sham + Ph and sham + Lig groups, uneven distribution with scattered staining resulting in reduced positive expression rate was observed for occludin and ZO-1 in both the D + Ph and D + Lig groups (Fig. 3C, $p<0.05$), suggesting that the intestinal barrier was damaged during aging.

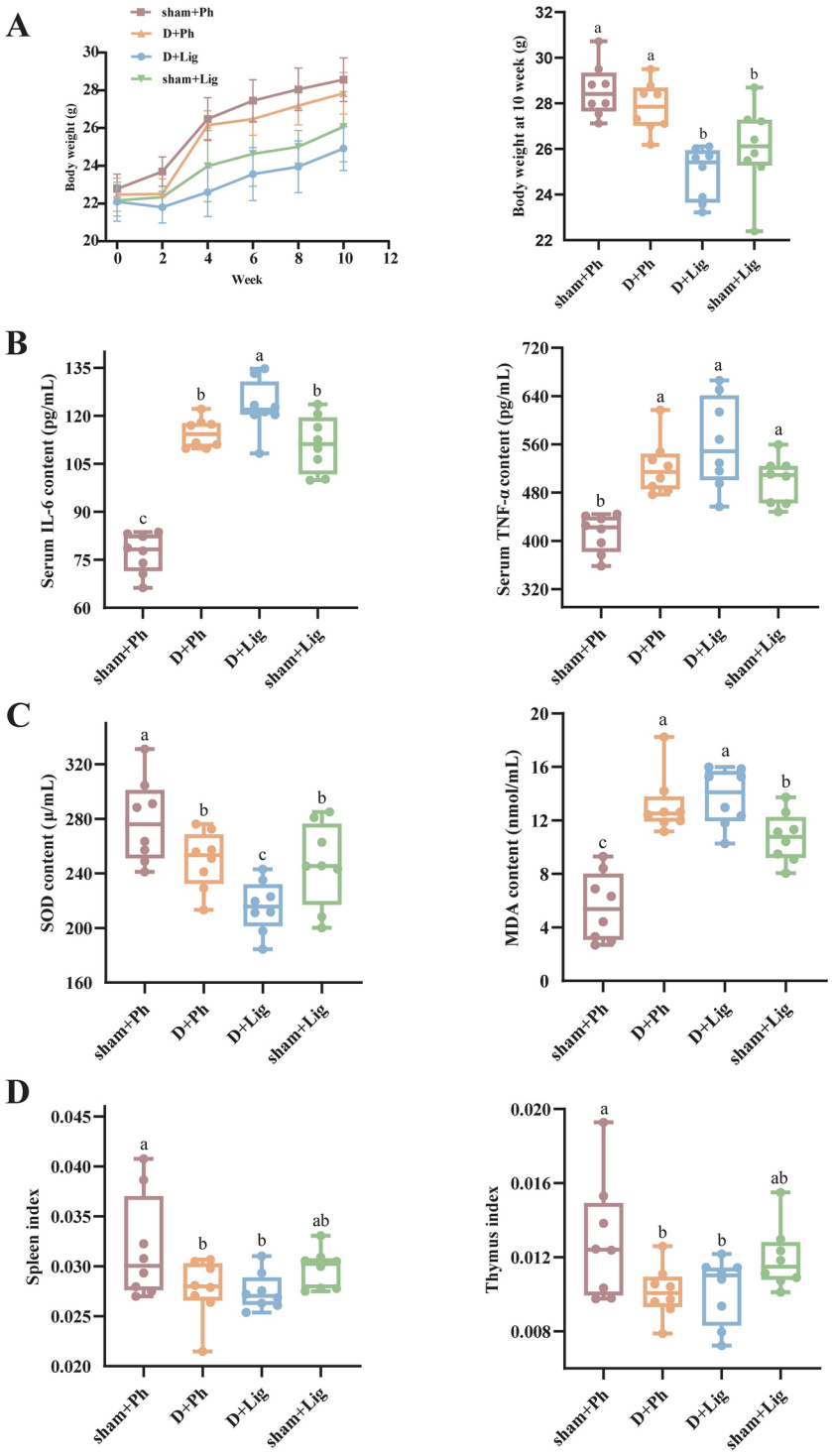

Fig. 2. D-gal-induced aging worsens the general state of periodontitis mice (n = 8/group). (**A**) Effects of aging on body weight, (**B**) Systemic inflammation levels of serum interleukin-6 (IL-6) and tumor necrosis factor alpha (TNF-α) content, (**C**) Oxidative stress levels of serum superoxide dismutase (SOD) and malonaldehyde (MDA) levels, (**D**) Immune organ indices of spleen and thymus. IL-6, interleukin-6; MDA, malonaldehyde; SOD, superoxide dismutase; TNF-α, tumor necrosis factor alpha.

Aging alters intestinal flora

To investigate the potential impact of D-gal-induced aging on the gut microbiota of periodontitis hosts, fecal samples were obtained for 16S rRNA sequencing. Species annotation was performed based on operational taxonomic unit (OTU) sequences. A total of 1,822 OTUs were identified, with 1,008 OTUs shared between

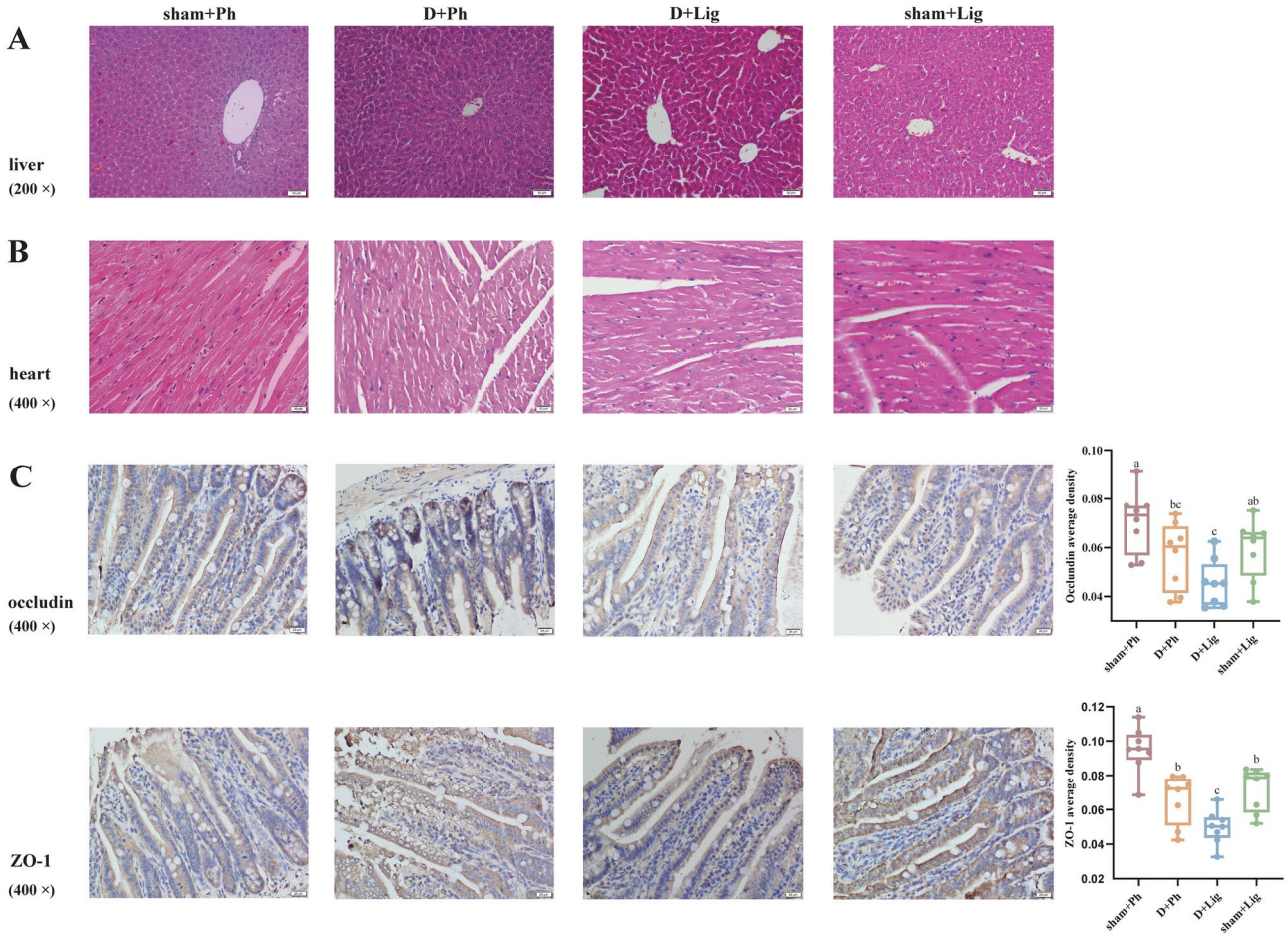

Fig. 3. D-gal-induced aging alters liver, heart and ileum status of periodontitis mice (n = 8/group). (**A**) Representative images of HE Staining of the liver tissues captured under a 200 × light microscope, (**B**) Representative images of HE Staining of the heart tissues captured under a 400 × light microscope, (**C**) Representative images of occludin and zonula occludens-1 (ZO-1) immunohistochemistry staining captured under a 400 × light microscope and average staining intensities. ZO-1, zonula occludens-1.

groups. The D + Lig group had 1,470 OTUs, with 198 OTUs unique. The sham + Lig group had 1,215 OTUs, with 92 exclusive. The D + Ph group had 1470 OTUs, with 207 OTUs unique (Fig. 4A).

Alpha diversity analysis was conducted to assess species diversity, evenness, and richness. The results indicate that Simpson, Shannon, ACE, and Chao1 indices were not significantly different between the D + Lig, sham + Lig and D + Ph groups (Fig. 4B). Principal coordinate analysis (PCoA) analysis based on the Bray Curtis distance revealed distinct clustering within each group, with an interaction region between the groups. The first principal coordinate (PC1) accounted for 25.28% of the variation, while the second principal coordinate (PC2) accounted for 15.92% (Fig. 4C). Analysis of similarities (ANOSIM) analysis indicated a significant difference between three groups, with R = 0.301 and $p = 0.001$ (Fig. 4D), suggesting clear dissimilarities in microbial composition. Furthermore, pairwise ANOSIM analysis revealed significant dissimilarities among the groups (Figure S1A). Further examination of the total relative abundance of the top 30 bacterial species at the phylum level using a heatmap revealed differences in microbial composition between groups (Fig. 4E, Figure S1B). The Firmicutes/Bacteroidetes (F/B) ratio was lower in the D + Lig group (0.456 ± 0.117) compared to the sham + Lig group (0.465 ± 0.070) and D + Ph group (0.571 ± 0.121).

Linear discriminant analysis effect size (LEfSe) analysis identified *Bacteroides*, *Levilactobacillus* and *Escherichia-Shigella* as biomarkers distinguishing between D + Lig and sham + Lig at the genus level, while Actinobacteria was at the phylum level (Fig. 4F). MetaStat analysis also revealed significant differences in flora at both the phylum and genus levels, comprising 7 and 46 taxa, respectively (Table S1). Noteworthy differences at the phylum level included WPS-2, Methylomirabilota, and Synergistota, while at the genus level, *Neisseria*, *Turicibacter*, and *Brachybacterium* were among the significantly different taxa. Phylum-level biomarkers for the D + Lig and D + Ph groups were identified as Actinobacteria and Verrucomicrobiota, with genus-level biomarkers including *Bacteroides*, *Lactobacillus*, *Acinetobacter*, *Akkermansia*, unidentified *Oscillospiraceae*, *Rikenella*, and *Leuconostoc* (Figure S1C). Detailed results of MetaStat analysis between the D + Lig and D + Ph groups can be found in Table S2.

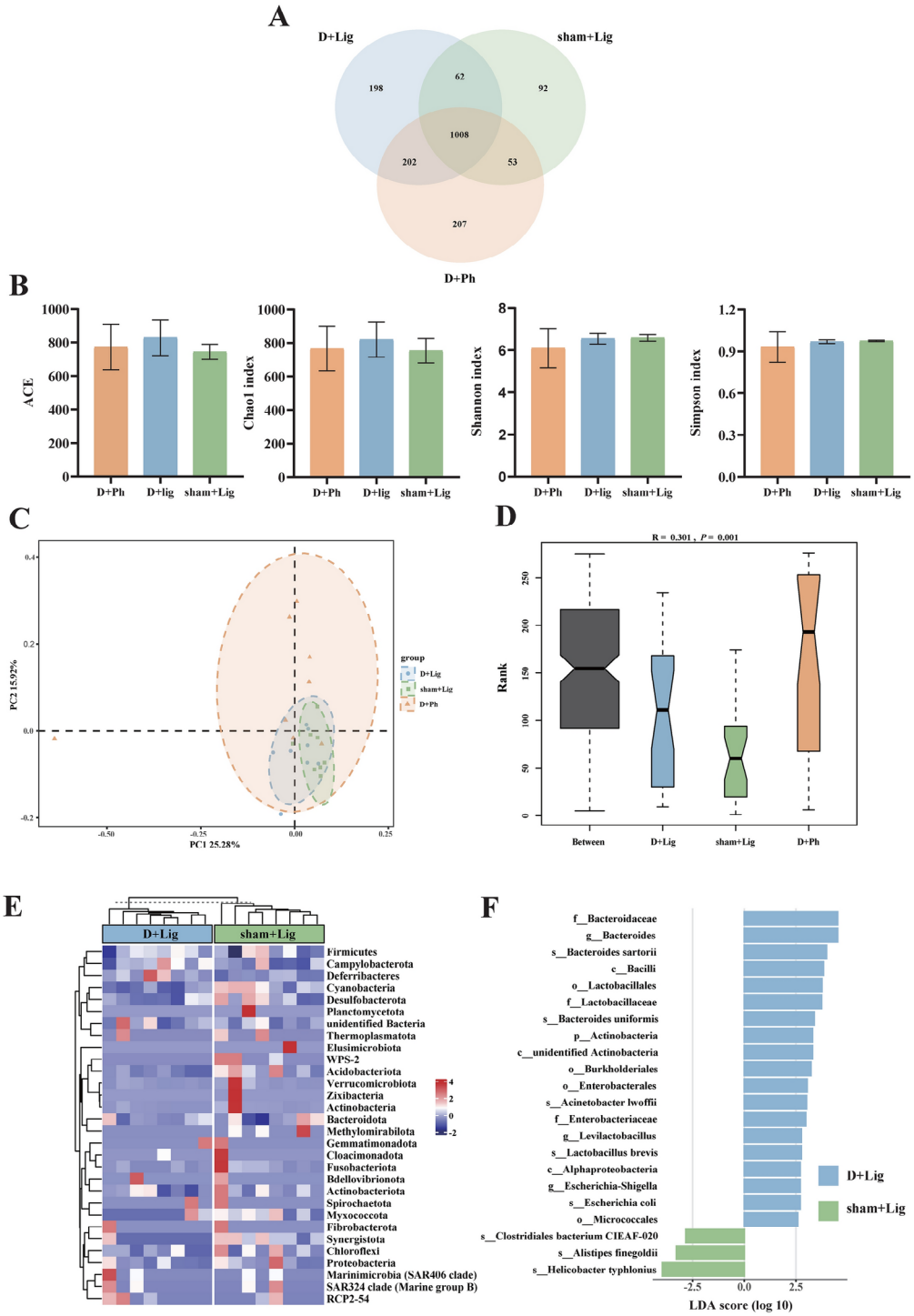

Fig. 4. D-gal-induced aging alters gut microbiota composition and structure in periodontitis mice (n = 8/group). (**A**) Veen diagram of operational taxonomic units (OTUs) among D + Ph, D + Lig and sham + Lig groups, (**B**) Alpha diversity -ACE, Chao1, Shannon and Simpson indices among D + Ph, D + Lig and sham + Lig groups, (**C**) Gut microbiota profiles were examined by principal coordinate analysis (PCoA) based on bray curtis distance among D + Ph, D + Lig and sham + Lig groups, (**D**) Analysis of similarities (ANOSIM) analysis was used to compare the composition of gut microbiota among D + Ph, D + Lig and sham + Lig groups. R > 0 indicates the difference of inter-group is greater than inner-group. The reliability of the statistical analysis was expressed as a *p*-value, (**E**) Heatmap of the gut microbiota at phylum level with relative abundance at top 30 in D + Lig and sham + Lig groups, (**F**) Linear discriminant analysis effect size (LEfSe) analysis showing the biomarkers of D + Lig and sham + Lig groups. Taxa with an linear discriminant analysis (LDA) score > 2.5 are shown. Bar graphs presented as mean ± standard deviation (SD). ANOSIM, analysis of similarities; LDA, linear discriminant analysis; LEfSe, linear discriminant analysis effect size; OTUs, operational taxonomic units; PCoA, principal coordinate analysis; SD, standard deviation.

Pearson's correlation coefficients was employed to evaluate the correlation between the abundance of the top 30 genera and physiological and biochemical indices (Fig. 5). *Bacteroides* exhibited a negative association with SOD level and intestinal barrier protein ZO-1 ($p < 0.05$). *Desulfovibrio* showed a positive association with osteoclast count, while *Lachnospiraceae* UCG-001 displayed a negative association ($p < 0.05$). Furthermore, *Lachnospiraceae* UCG-001 exhibited a positive correlation with the thymus index and ZO-1 ($p < 0.05$). While *Lactobacillus*, [*Eubacterium*] *siraeum* group and *Ralstonia* showed a positive correlation with inflammatory factor including TNF-α level, while unidentified *Oscillospiraceae* showed a negative association with IL-6 ($p < 0.05$).

Periodontitis-related fecal metabolites enriched during aging

PCoA and partial least squares discriminant analysis (PLS-DA) analyses were conducted on the three groups to investigate altered metabolic profiles. The PC1 accounted for 30.41% and the PC2 accounted for 20.31% of the variation (Fig. 6A ~ B). The volcano plot demonstrated differential metabolites between groups. In the comparison between the D + Lig and sham + Lig groups, D-gal-induced aging significantly altered 57 metabolites in mice with periodontitis, with 39 metabolites showing increased abundance and 18 metabolites showing a decrease (Fig. 6C, Table S3). Metabolite annotation using the HMDB databases revealed that 32 metabolites could not be annotated at the SuperClass level. The remaining 25 metabolites were classified as Lipids and lipid-like molecules (21.05%), Organic acids and derivatives (14.04%), and Benzenoids (3.51%). Nucleosides, nucleotides, and analogues; Organic oxygen compounds; and Phenylpropanoids and polyketides each accounted for 1.75% (Fig. 6D). In contrast, periodontitis altered 55 metabolites between D + Lig and D + Ph groups, with 31 metabolites up-regulated and 24 metabolites down-regulated (Figure S2A, Table S4). The HMDB databases classified these 32 metabolites as Lipids and lipid-like molecules (20.00%), Organic oxygen compounds (3.64%), Phenylpropanoids and polyketides (7.27%), Organoheterocyclic compounds (9.09%), Organic acids and derivatives (10.91%), and Benzenoids (7.27%) (Figure S2B). The heatmap depicted the inter-

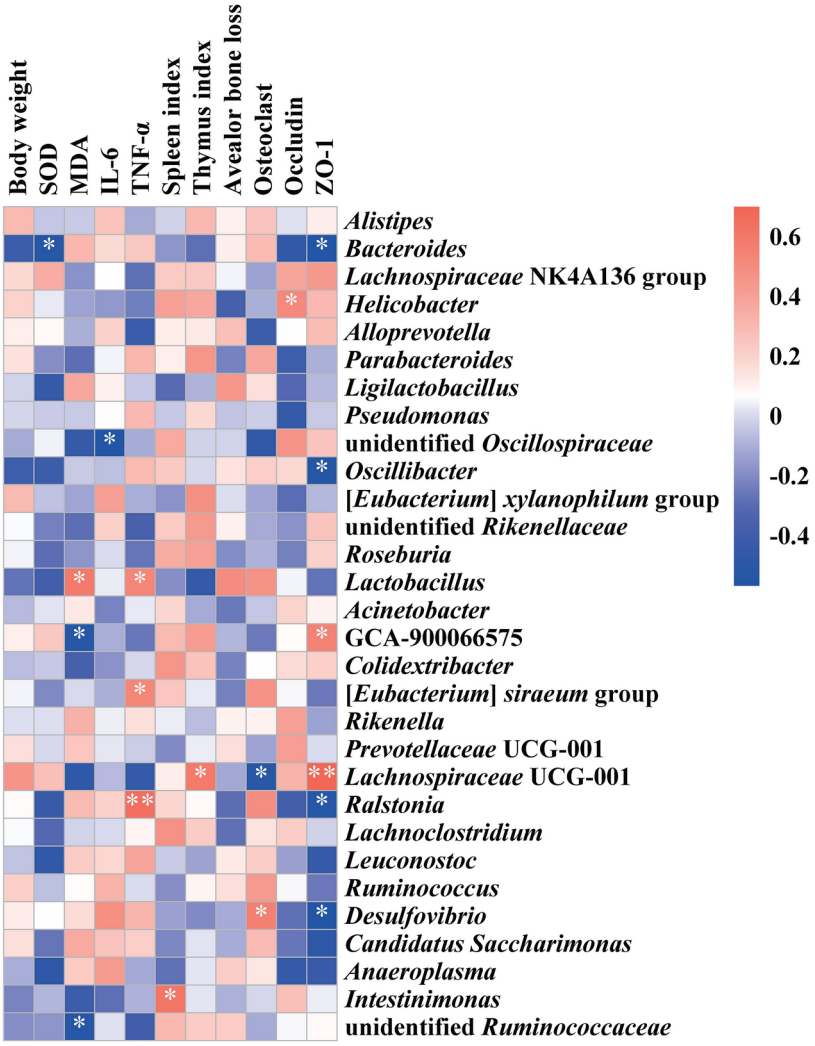

Fig. 5. Pearson's correlation coefficients between the top 30 gut microbes at genus level and physiological indicators. */**, represents the correlation was statistically significant, * $p < 0.05$, ** $p < 0.01$.

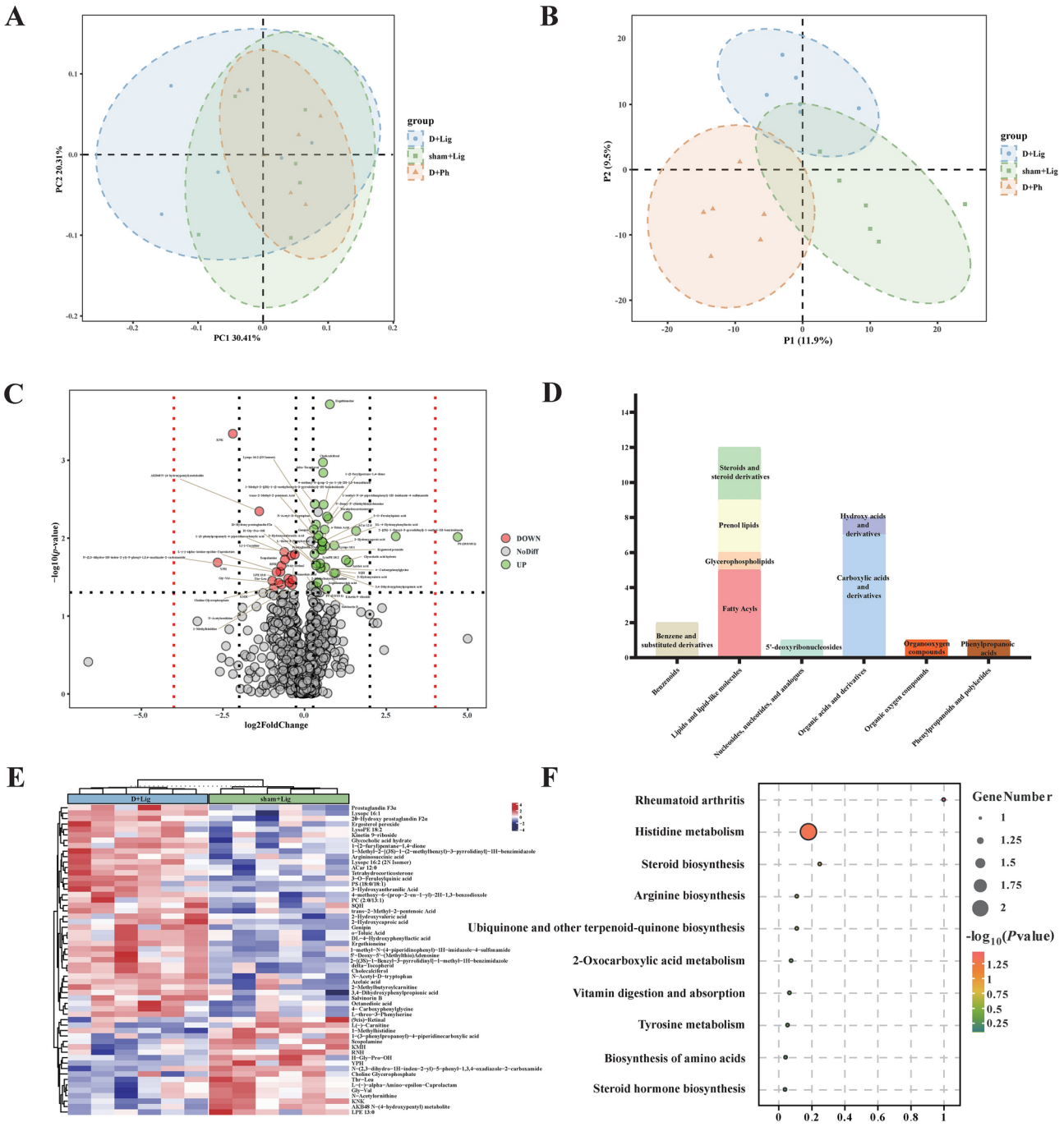

Fig. 6. Differences of gut metabolomic profiles with D-gal-induced aging process (n = 6/group). (**A**) Differential metabolites in D + Ph, D + Lig and sham + Lig groups were examined by PCoA based on bray curtis distance, (**B**) Partial least squares discriminant analysis (PLS-DA) score of fecal metabolite profiles among D + Ph, D + Lig and sham + Lig groups, (**C**) Volcanic map shows that 57 differentially accumulated [$\log_2$(FoldChange) on the x-axis] and significantly altered [- $\log_{10}$(*p*-value) on y-axis] metabolites between D + Lig and sham + Lig groups, (**D**) The proportion of differential fecal metabolite categories associated with aging in D + Lig and sham + Lig groups, (**E**) Heatmap of significantly different metabolites between D + Lig and sham + Lig groups, (**F**) Kyoto encyclopedia of genes and genomes (KEGG) pathway enrichment scatter plot showing age-related changes in fecal metabolism between D+Lig and sham+Lig groups. KEGG, kyoto encyclopedia of genes and genomes; PLS-DA, partial least squares discriminant analysis.

and intra-group differences and clustering of these differential metabolites (Fig. 6E, Figure S2C). To explore the potential functions of these differentially expressed metabolites, a kyoto encyclopedia of genes and genomes (KEGG) enrichment analysis was conducted. Unfortunately, only a portion of these differential metabolites were annotated in the database. The most significantly enriched pathways altered by D-gal-induced aging included

rheumatoid arthritis and histidine metabolism (Fig. 6F), while periodontitis primarily influenced Estrogen signaling pathway (Figure S2D).

Finally, the relationship between gut microbiota composition and metabolites in the context of D-gal-induced aging was further investigated. Pearson's correlation analysis was performed on the top 20 differentially abundant bacteria at the genus level along with the top 36 differentially expressed metabolites in two ion modes between group D + Lig and sham + Lig (Fig. 7). D-gal-induced aging primarily impacts amino acid synthesis and metabolism, particularly histidine, arginine, and tyrosine, which are associated with increased levels of Ergothioneine and 3,4-Dihydroxyphenylpropionic acid, as well as decreased levels of N-Acetylornithine and 1-Methylhistidine. Ergothioneine exhibited significant positive correlations with *Delftia*, *Sphingomonas*, *Lysinibacillus*, *Turicibacter* and *Thermovirga*, among others, while 3,4-Dihydroxyphenylpropionic acid only be found to positive with *Butyricimonas* ($p < 0.05$). Although not statistically significant, there was a negative correlation between N-Acetylornithine and most genera. Additionally, periodontitis affected amino acid metabolism, mainly related to differential metabolites such as L-Threonine, Urocanic acid, and Ergothioneine.

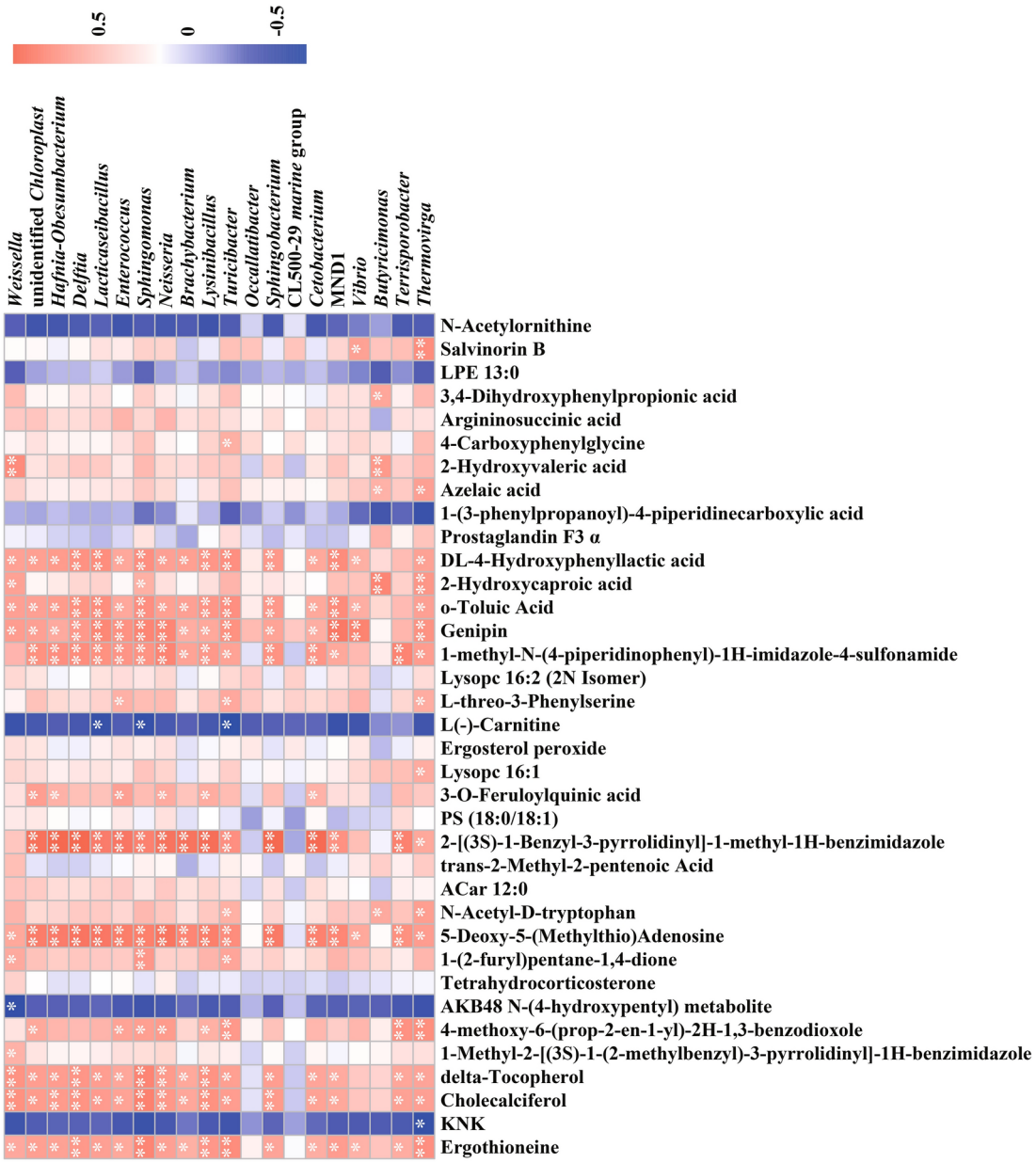

Fig. 7. Pearson's correlation coefficients between the abundance of the top 20 differential enriched gut bacteria at genus levels (top) and the abundance of the top 36 differential metabolites between D + Lig and sham + Lig groups (16 metabolites in negative ion mode on the top side, 20 metabolites in positive ion mode on the bottom). The correlation effect is represented by a color gradient from blue (negative correlation) to red (positive correlation).

Ergothioneine exhibits a significant positive correlation with *Lactobacillus* and a negative correlation with *Subgroup* 23 ($p < 0.05$) (Figure S3).

Discussion

Aging is a notable risk factor for increased susceptibility to periodontal disease[22]. This study demonstrated that D-gal-induced aging is accompanied by various alterations in clinical, physiological, biochemical, and intestinal microecology parameters. Among these factors, gut microbiota and its metabolites play crucial roles in mediating age-related changes in periodontal diseases.

Alveolar bone resorption is a significant marker for the progression of periodontitis. In this study, we found that D-gal-induced aging exacerbates osteoclastogenesis, decreases alveolar bone height, and correlates with increased inflammation levels and deeper periodontal pocket (Fig. 1). These findings align with previous research indicating that both natural aging and accelerated aging mice exhibited age-related bone loss in the alveolar or lower limb bones, characterized by irregular thinning of trabecular bone and degradation of collagen fibrils[23–26]. Additionally, in vitro studies have shown that senescence in bone marrow-derived mesenchymal stem cells (BMSCs) impairs their proliferative capacity and paracrine function, leading to bone loss and osteoporosis[27].

The administration of D-gal is a well-established method for effectively simulating the natural aging, and is commonly used to induce age-related changes across various systems, including locomotor, nervous, digestive, and cardiovascular systems[28–32]. In this study, D-gal-treated mice exhibited a gradual deceleration in body weight growth with accelerated aging, whereas weight gain was significantly greater in periodontally healthy, senescent mice compared to those with periodontitis. D-gal-induced aging also led to elevated levels of pro-inflammatory cytokines, such as IL-6 and TNF-α (Fig. 2), creating an imbalance between anti-inflammatory and pro-inflammatory factors that exacerbates the aging process. Furthermore, aging resulted in damage to immune organs, compromising their infection-fighting capabilities[33]. Our findings also indicate elevated oxidative stress in the aging mice, as evidenced by decreased SOD activity and increased MDA levels (Fig. 2). Oxidative stress inhibits bone formation and promotes bone resorption by affecting osteocyte signal pathways[34]. Increased osteoclast activity in osteoporosis is linked to elevated ROS production, with MDA serving as a reliable indicator for osteoclast activities[35], while SOD helps mitigate oxidative damage and counteracts ROS-mediated bone resorption[36]. Additionally, aging has been found to increase intestinal permeability[37]. The junction proteins ZO-1 and occludin are crucial to maintaining intestinal barrier function, and our results reaffirm the association between reduced levels of these proteins and age-related intestinal barrier (Fig. 3)[38,39].

To investigate the impact of gut microbiota in D-gal-induced aging process, the D + Lig, sham + Lig, and D + Ph groups were selected to analyze intestinal flora using 16S rRNA sequencing. Our results demonstrated that aging not only exacerbates the phenotype of periodontitis but also affects the intestinal microenvironment. Interestingly, there were no significant differences in the alpha diversity of intestinal flora among the groups. This may be attributed to the fact that periodontitis can interfere with saliva and gut microbiota[40], and the ambiguous relationship between D-gal-induced aging and gut microbiota diversity[41–45]. Based on LEfSe result, we identified *Bacteroides*, *Levilactobacillus*, and *Escherichia-Shigella* as genus-level biomarkers for age-related periodontitis mice, while Actinobacteria was identified as a phylum-level biomarker (Fig. 4). Additionally, Actinobacteria and Verrucomicrobiota were found to be phylum-level biomarkers distinguishing the D + Lig and D + Ph groups (Figure S1). Actinobacteria has been suggested as a marker of aging, with its abundance increasing in the intestinal bacteria of elderly individuals compared to younger mice[37,46,47], and its metabolites, which are involved in carbohydrate metabolism, may contribute to modifying cognitive functions, including Alzheimer's disease through the gut-brain axis[48]. *Escherichia-Shigella* produces metabolites such as propionate ester, which stimulate the formation of osteoclasts, impede the proliferation of osteoblasts, and hinder bone growth[49]. Furthermore, *Bacteroides* was found to be significantly enriched in the gut of aging mice and older adults following weight loss[44,50]. *Bacteroides* and *Levilactobacillus* belong to Bacteroidetes and Firmicutes, respectively, produce propionic acid, which inhibits hepatic gluconeogenesis and cholesterol synthesis[51]. Our MetaStat analysis also revealed an increase in seven phylum-level bacteria associated with aging. Among these, Fusobacteriota, including the genus *Fusobacterium*, and Synergistota, were found to be enriched in the subgingiva of periodontitis[52,53]. This enrichment of oral microbiota in the gut may be attributed to age-related impairment of gut barrier structure and functiong, allowing for the colonization of oral microbiota through ingestion. At the genus level, aging significantly altered 46 species of gut microbiota, of which 43.48% belonged to Firmicutes and 6.52% to Bacteroidetes (Table S1). Firmicutes and Bacteroidetes make up about 90% of the intestinal flora[54] and play pivotal roles in regulating the expression of osteoclast genes[55]. The F/B ratio changes across different life stages, with low, high and low ratios observed in infants, adults, and the elderly, respectively[56]. In our study, the F/B ratio decreased in the D + Lig group, showing a similar tendency[38,44,57]. Moreover, the F/B ratio impacts the synthesis of short-chain fatty acids (SCFAs), such as formate, acetate, propionate, butyrate, and others, which play diverse biological roles[58]. For instance, butyrate and propionate have been shown to exert anti-inflammatory effects in periodontitis by inhibiting the expression of inflammation-related factor[59,60]. Gut microbes exert their influence on the physiological status of the elderly through various biomolecules, nutrient signaling, and epigenetic mechanisms[61]. These findings may explain the observed changes in the D + Lig mice in our study (Fig. 5).

To further explore the microbe-host interaction mechanisms affecting periodontitis in D-gal-induced aging, we conducted fecal metabolome analysis. Our findings indicated that the most prominent differential metabolites in D-gal-induced aging model were lipids and lipid-like molecules, including fatty acyls, glycerophospholipids, prenol lipids, steroids and steroid derivatives. These compounds are crucial not only as structural components of cells and energy sources but also in regulating inflammatory responses, cellular senescence, and metabolic disorders[62]. Aging-induced abnormalities in lipid metabolism elevate the risk of bone disease, potentially due to mitochondrial dysfunction, oxidative stress, osteocyte apoptosis, autophagy disorder,

and hormone level modulation associated with lipid molecules[63–65]. Moreover, disrupted lipid metabolism is prevalent in periodontitis, where inflammatory response mediated by this aberrant metabolism contribute to the severity of periodontal disease[66,67]. Furthermore, we identified second significant changes in the synthesis and metabolism of amino acid, specifically histidine, arginine, and tyrosine (Fig. 6). Aging results in a decline in systemic metabolic efficiency and abnormal amino acid metabolism, leading to elevated homocysteine (Hcy) level, which is positively correlated with alveolar bone destruction[68,69]. Histamine, essential for regulating inflammation, immunity and digestion, can aggravate periodontal inflammation and ABL through the NLRP3/Caspase-1 pathway when deficient[70]. Additionally, arginine, an essential amino acid, is converted to citrulline via the NADPH pathway, facilitating nitric oxide (NO) synthesis. However, excessively high NO can be cytotoxic to alveolar bone[71]. Previous studies have linked D-gal-induced aging to disturbances in glucose and lipid metabolism, oxidative damage, accumulation of advanced glycation end products, apoptosis, and insulin resistance, with glucose and lipid metabolism disorder being particular significant[72,73]. Metabolomic analysis based on plasma and liver have shown that naturally aged mice exhibit metabolic alterations primarily in amino acid and fat metabolism, affecting various differential pathways including signal transduction, immune system, amino acid metabolism, carbohydrate metabolism, lipid metabolism, cancer, cell growth and death[74,75]. The findings are consistent with our current study and suggest that D-gal administration does not significantly interfere with the basal metabolism of mice and reflects some of the metabolic profile changes associated with aging.

Conclusion

This study investigated the impact of D-gal-induced senescence on periodontal symptoms and the intestinal microenvironment. The findings suggest that aging exacerbates the degeneration of periodontal supporting tissues, intensifies inflammation, and reduces immune function. Furthermore, aging alters the composition and structure of gut microbiota, resulting in a reduced F/B ratio. Specifically, *Bacteroides*, *Levilactobacillus*, and *Escherichia-Shigella* are identified as genus-level biomarkers of aging-periodontitis mice. Additionally, aging induces lipid metabolic disorders in mice with periodontitis, potentially through rheumatoid arthritis and histidine metabolism pathways. However, the present study is subject to certain limitations, including the absence of natural aging mice as controls and the lack of validation of the upstream and downstream signals associated with the identified pathways. Future research should incorporate natural aging models to gain a more comprehensive understanding of the dynamic changes occurring in alveolar bone during the aging process.

Methods

Experimental animals and grouping

Thirty-two male C57BL/6 J specific pathogen-free (SPF) mice, aged 8 weeks and weighing between 18-20 g, were obtained from Hunan SJA Laboratory Animal Co., Ltd, Chang Sha, China. The mice were subject to the experiment after undergoing an acclimatization period. The study was approved by the Institutional Animal Management Committee of Zunyi Medical University (Identification Code: ZYLS [2021]1–046) and conducted following national and institutional regulations on animal experimentation.

After adaptive feeding, the 32 mice were divided into four groups. They are designated respectively as sham + Ph (sham + periodontal health) group, D + Ph (D-gal + periodontal health) group, D + Lig (D-gal + ligation) group, and sham + Lig (sham + ligation) group. Group D + Lig and D + Ph were received subcutaneous injections of 10% D-gal (Solarbio, China) solution at a dose of 500 mg/kg from day 0 to the 10th week. Group sham + Ph and sham + Lig were subcutaneously injected with an isodose phosphate-buffered saline (PBS) solution as a control. After 2 weeks of D-gal or PBS injection, the mice were anesthetized with 0.3% pentobarbital sodium at a dose of 0.1 ~ 0.2 ml/10 g prior to undergoing periodontal surgery. Both D + Lig and sham + Lig groups underwent ligation with 5–0 silk thread at the neck of the bilateral maxillary second molars to induce experimental periodontitis. The ligature was inspected every 2 days to ensure the integrity of the periodontium and replaced promptly if it fell off.

Collection of experimental samples

The body weight of mice was recorded weekly throughout the study. At the end of the study, the mice were administered 0.3% pentobarbital sodium at a dose of 0.1 ~ 0.2 ml/10 g, and euthanized by spinal cord dislocation method. Samples began to collect 12 h after the last subcutaneous injection of D-gal. Fecal samples were collected by natural collection and stimulated defecation, and then rapidly frozen by liquid nitrogen and stored at -80 °C until further detection. Blood samples were collected from eyeballs under anesthesia, then centrifuged at 3000 rpm and 4 °C for 10 min to obtain serum, which was subsequently stored at − 80°C for further use. After blood collection, the mice were euthanized. Maxillary tissue blocks were taken from one side of the mice and fixed with 4% paraformaldehyde for 48 h. These tissue blocks were then decalcified in a 10% EDTA solution until pins could be inserted into the bone tissue without resistance. Once decalcification was complete, the tissue blocks were embedded in paraffin for further analysis. The alveolar bone on the opposite side was cleared of soft tissue, immersed in 3% hydrogen peroxide overnight, cleansed with 97% alcohol, and subsequently stained using a 0.1% methylene blue solution. Additionally, the heart, liver, and ileum tissues were fixed in 4% paraformaldehyde for 48 h, followed by dehydration and embedded in paraffin.

Thymus and spleen indices

The body weight of mice was measured before sacrifice. Spleen and thymus tissues were dissected intact, and washed with precooled PBS, and the surface fluid was blotted dry with absorbent paper and then weighed.

Oxidative stress and inflammatory factors detection

Biochemical kits (Nanjing Jiancheng, China) were used to measure serum SOD and MDA activities, while Enzyme-Linked Immunosorbent Assay (ELISA) kits (Jianglai, China) were utilized to measure serum IL-6 and TNF-α levels. The experimental procedures strictly followed the instructions provided by the kit manufacturers.

Histological analysis

The pathological changes in periodontal tissues, heart, and liver were observed through hematoxylin–eosin (HE) staining, finally examined under light microscopy at 100×, 200× or 400× depending on the specific tissues.

Immunohistochemistry staining was employed to detect the expression of tight junction proteins of ileum sections, including occludin and ZO-1. The integrated optical density (IOD) value of the ileum tissues using Image Pro Plus software. After calibration, the IOD value was normalized by the measured area to represent protein expression levels. This process was repeated three times to obtain an average value.

Methylene blue staining was conducted on the maxillary molar area, and the alveolar bone was fixed and examined under a stereoscopic microscope. The linear ABL was determined by measuring the distance from the cemento-enamel junction to the apex of the alveolar bone at six specific sites around the second molar: mesio-buccal, buccal, disto-buccal, mesio-palatal, palatal and disto-palatal. These measurements at the six sites were then averaged to obtain the ABL value of the second molar.

Osteoclasts in the region of the second molar were stained using a tartrate-resistant acid phosphatase (TRAP) staining kit (Solarbio, China). Subsequently, the periodontal region of the maxillary second molar was examined, and six randomly selected non-overlapping fields were used for counting TRAP-positive multinucleated cells. Specifically, large multinucleated TRAP-positive cells located near the bone surface within bone lacunae were enumerated.

16S rRNA sequencing and analysis

The magnetic bead method was employed for the extraction of total fecal DNA, which served as a template for V4 region sequencing (Tiangen Biotech, China). Bac library construction and computerized data processing were carried out using the Illumina NovaSeq6000 sequencing platform (Beijing, China). And FLASH 1.2.7 was utilized for quality control of raw sequencing data. OTUs were selected through 97% consensus clustering with the Uparse algorithm (V7.0.1), and OTU sequences with the highest frequency of occurrence were chosen as representative sequences. Then the sequences were annotated by Mothur and SSUrRNA databases from SILVA138.

To analyze differences in alpha diversity between groups, Shannon, Simpson and Chao1 indices were calculated using Qiime V1.9.1. Bray Curtis distance was computed to determine beta diversity, which was further analyzed through PCoA and ANOSIM analysis. For analysis at the phylum level, a heatmap of the top 30 absolute abundance bacteria based on relative abundance was generated using the Heatmap package of R. Biomarkers were employed utilizing LEfSe, with an linear discriminant analysis (LDA) score > 2.5 and $p < 0.05$ considered statistically significant. Significant bacterial colonies at both phylum and genus levels were analyzed by applying the Metastats method with $p < 0.05$. Furthermore, Pearson correlation analysis explored potential relationships between dominant genera and physiological indicators. Data visualization was conducted using R4.2.1.

Untargeted metabolomic analysis

100 mg fecal samples were mixed with a precooled 500 µl 80% aqueous methanol solution and vigorously vortexed. The mixture was then placed in an ice bath for 5 min and centrifuged at 15,000 g and 4 ℃ for 20 min. The resulting supernatant was then mixed with mass LC–MS-grade water to achieve a methanol concentration of 53%, and another round of centrifugation for 20 min, then collect supernatant for LC–MS/MS analysis. An equal volume of feces from each sample was combined to create Quality control (QC) sample. The fecal samples were replaced with a solution containing a methanol concentration of 53% as a blank sample. LC–MS/MS analysis was conducted by Novogene Co., Ltd. (Beijing, China). Ultimately, the metabolites were quantified.

The software metaX was utilized for data transformation and conducting PCoA and PLS-DA to investigate changes in metabolic profiles among different groups. The *t*-test was employed to calculate the *p*-value between the two groups of metabolites. Metabolites with variable importance in projection (VIP) > 1.0, *p*-value < 0.05, and $|\log_2\text{Fold Change}| \geq 0.263$ were considered as criteria for screening differential metabolites. A volcano plot illustrating differential metabolites was generated using three parameters: the VIP value, $\log_2$(Fold Change), and $-\log_{10}$(*p*-value). Heatmaps depicting differential metabolites were used Heatmap package of R. The KEGG database, the HMDB database, along with the LIPIDMaps database were utilized for annotating these differential metabolites. The KEGG database was also used to study the functions and metabolic pathways of metabolites. Notably, significant enrichment of this pathway was observed at a significance level of 0.05. The top differential metabolites in both positive and negative ion modes were selected alongside the top differential bacterial genera for further analysis. The Pearson correlation coefficient was calculated by corrplot in R4.2.1.

Statistical analysis

The data were analyzed using Statistical Product and Service Solutions (SPSS, International Business Machine Inc, USA) 29.0, and all quantitative data were presented as mean ± standard deviation (SD). *T*-test was employed for comparing two groups with measurement data conforming to normal distribution and homogeneity of variance, while one-way ANOVA was used for comparing multiple groups. Non-parametric tests were utilized for non-normally distributed data. A two-tailed $p < 0.05$ was considered statistically significant.

Ethics statement

This project has been approved by the Institutional Animal Management Committee of Zunyi Medical University (Identification Code: ZYLS [2021]1–046) and all the experiments were safeguarded the well-being of experimental animals, and adhered to ethical principles. And all the authors complied with the ARRIVE guidelines.

Data availability

The raw data of 16S rRNA-seq regarding this study were submitted to NCBI Sequence Read Archive under Bioproject ID PRJNA1091075. Additionally, the metabolomics data were submitted to the OMIX, China National Center for Bioinformation / Beijing Institute of Genomics, Chinese Academy of Sciences (https://ngdc.cncb.ac.cn/omix: accession no. OMIX007281).

Received: 27 March 2024; Accepted: 9 October 2024
Published online: 30 October 2024

References

1. Partridge, L., Deelen, J. & Slagboom, P. E. Facing up to the global challenges of ageing. *Nature* **561**, 45–56 (2018).
2. Villalobos, V. et al. Aging envisage imbalance of the periodontium: A keystone in oral disease and systemic health. *Front. Immunol.* **13**, 1044334 (2022).
3. Persson, G. R. Dental geriatrics and periodontitis. *Periodontol 2000*, **74**, 102–115 (2017).
4. Persson, G. R. Periodontal complications with age. *Periodontol 2000*, **78**, 185–194 (2018).
5. Eke, P. I. et al. Periodontitis prevalence in adults >/= 65 years of age, in the USA. *Periodontol 2000*, **72**, 76–95 (2016).
6. Genco, R. J. & Sanz, M. Clinical and public health implications of periodontal and systemic diseases: An overview. *Periodontol 2000*, **83**, 7–13 (2020).
7. Barbe-Tuana, F., Funchal, G., Schmitz, C. R. R., Maurmann, R. M. & Bauer, M. E. The interplay between immunosenescence and age-related diseases. *Semin. Immunopathol.* **42**, 545–557 (2020).
8. Elsayed, R. et al. Microbially-induced exosomes from dendritic cells promote paracrine immune senescence: novel mechanism of bone degenerative disease in mice. *Aging Dis.* **14**, 136–151 (2023).
9. Elsayed, R. et al. Porphyromonas gingivalis provokes exosome secretion and paracrine immune senescence in bystander dendritic cells. *Front. Cell Infect. Microbiol.* **11**, 669989 (2021).
10. Gonzalez-Osuna, L. et al. Premature senescence of T-cells favors bone loss during osteolytic diseases. a new concern in the osteoimmunology arena. *Aging Dis.* **12**, 1150–1161 (2021).
11. Gonzalez-Osuna, L. et al. Senescent $CD4^{(+)}CD28^{(-)}$ T lymphocytes as a potential driver of Th17/Treg imbalance and alveolar bone resorption during periodontitis. *Int. J. Mol. Sci.* **23**, 2543 (2022).
12. Cai, N., Wu, Y. & Huang, Y. Induction of accelerated aging in a mouse model. *Cells* **11**, 1418 (2022).
13. Azman, K. F., Safdar, A. & Zakaria, R. D-galactose-induced liver aging model: Its underlying mechanisms and potential therapeutic interventions. *Exp. Gerontol.* **150**, 111372 (2021).
14. Azman, K. F. & Zakaria, R. D-Galactose-induced accelerated aging model: an overview. *Biogerontology* **20**, 763–782 (2019).
15. Sczepanik, F. S. C. et al. Periodontitis is an inflammatory disease of oxidative stress: We should treat it that way [J]. *Periodontol 2000*, **84**, 45–68 (2020).
16. Tatge, L., Solano Fonseca, R. & Douglas, P. M. A framework for intestinal barrier dysfunction in aging. *Nat. Aging* **3**, 1172–1174 (2023).
17. Kuhn, F. et al. Intestinal alkaline phosphatase targets the gut barrier to prevent aging. *JCI Insight* **5**, e134049 (2020).
18. Han, N. et al. The impacts of oral and gut microbiota on alveolar bone loss in periodontitis. *J. Periodontal. Res.* **58**, 1139–1147 (2023).
19. Shahi, S.K., Zarei, K., Guseva, N.V., Mangalam, A.K. Microbiota Analysis Using Two-step PCR and Next-generation 16S rRNA Gene Sequencing [J]. *J Vis Exp*, **15**. https://doi.org/10.3791/59980 (2019).
20. Wang, W. J. et al. Characterizing the composition of intestinal microflora by 16S rRNA gene sequencing. *World J. Gastroenterol.* **26**, 614–626 (2020).
21. Cui, L., Lu, H. & Lee, Y. H. Challenges and emergent solutions for LC-MS/MS based untargeted metabolomics in diseases. *Mass Spectrom Rev.* **37**, 772–792 (2018).
22. Colombo, A. P. & Wu, B. Aging and Oral Health: Biological and Sociobehavioral Perspectives. *J. Dent. Res.* **102**, 841–843 (2023).
23. Clark, D. et al. The contribution of macrophages in old mice to periodontal disease. *J. Dent. Res.* **100**, 1397–1404 (2021).
24. Bertolini, M. & Clark, D. Periodontal disease as a model to study chronic inflammation in aging. *Geroscience* **46**, 3695–3709 (2024).
25. Imerb, N. et al. D-galactose-induced aging aggravates obesity-induced bone dyshomeostasis. *Sci. Rep.* **12**, 8580 (2022).
26. Zhang, F. et al. Diallyl trisulfide ameliorates bone loss and alters specific gut microbiota and serum metabolites in natural aging mice. *Food Funct.* **14**, 7642–7653 (2023).
27. Liu, F. et al. S-sulfhydration of SIRT3 combats BMSC senescence and ameliorates osteoporosis via stabilizing heterochromatic and mitochondrial homeostasis. *Pharmacol. Res.* **192**, 106788 (2023).
28. Nie, L. et al. Tetramethylpyrazine Nitrone alleviates D-galactose-induced murine skeletal muscle aging and motor deficits by activating the AMPK signaling pathway. *Biomed. Pharmacothe.r* **173**, 116415 (2024).
29. Wang, X. et al. Codonopsis pilosula water extract delays D-galactose-induced aging of the brain in mice by activating autophagy and regulating metabolism. *J. Ethnopharmacol.* **327**, 118016 (2024).
30. Aon-Im, P. et al. Evaluation of the Impact of Alternanthera philoxeroides (Mart.) Griseb. Extract on Memory Impairment in D-Galactose-Induced Brain Aging in Mice through Its Effects on Antioxidant Enzymes, Neuroinflammation, and Telomere Shortening. *Molecules* **29**, 503 (2024).
31. Shen, L. et al. Cow placenta extract ameliorates d-galactose-induced liver damage by regulating BAX/CASP3 and p53/p21/p16 pathways. *J. Ethnopharmacol.* **323**, 117685 (2024).
32. Wang, S. S. et al. D-galactose-induced cardiac ageing: A review of model establishment and potential interventions. *J. Cell Mol. Med.* **26**, 5335–5359 (2022).
33. Liu, J. et al. Immune senescence and periodontitis: From mechanism to therapy. *J. Leukoc. Biol.* **112**, 1025–1040 (2022).
34. Kimball, J. S., Johnson, J. P. & Carlson, D. A. Oxidative Stress and Osteoporosis. *J. Bone Joint Surg. Am.* **103**, 1451–1461 (2021).
35. Zhao, F., Guo, L., Wang, X. & Zhang, Y. Correlation of oxidative stress-related biomarkers with postmenopausal osteoporosis: a systematic review and meta-analysis. *Arch. Osteoporos.* **16**, 4 (2021).
36. Wang, H. et al. BNTA alleviates inflammatory osteolysis by the SOD mediated anti-oxidation and anti-inflammation effect on inhibiting osteoclastogenesis. *Front. Pharmacol.* **13**, 939929 (2022).

37. Gong, C. X. et al. Gastrodia elata and parishin ameliorate aging induced "leaky gut" in mice: Correlation with gut microbiota. *Biomed. J.* **46**, 100547 (2023).
38. Gao, Y. et al. Lactobacillus plantarum Y44 alleviates oxidative stress by regulating gut microbiota and colonic barrier function in Balb/C mice with subcutaneous d-galactose injection. *Food Funct.* **12**, 373–386 (2021).
39. Li, H. et al. Blueberry-mulberry extract alleviates cognitive impairment, regulates gut metabolites, and inhibits inflammation in aged mice. *Foods* **12**, 860 (2023).
40. Xue, L. et al. Chronic periodontitis induces microbiota-gut-brain axis disorders and cognitive impairment in mice. *Exp. Neurol.* **326**, 113176 (2020).
41. Luo, D. et al. Gut microbiota combined with metabolomics reveals the metabolic profile of the normal aging process and the anti-aging effect of FuFang Zhenshu TiaoZhi(FTZ) in mice. *Biomed. Pharmacother.* **121**, 109550 (2020).
42. Li, L. et al. Fructus Ligustri Lucidi preserves bone quality through the regulation of gut microbiota diversity, oxidative stress, TMAO and Sirt6 levels in aging mice. *Aging (Albany NY)* **11**, 9348–9368 (2019).
43. Alam, M. S., Gangiredla, J., Hasan, N. A., Barnaba, T. & Tartera, C. Aging-Induced Dysbiosis of Gut Microbiota as a Risk Factor for Increased Listeria monocytogenes Infection. *Front. Immunol.* **12**, 672353 (2021).
44. He, W. et al. Beneficial effect of GABA-rich fermented milk whey on nervous system and intestinal microenvironment of aging mice induced by D-galactose. *Microbiol. Res.* **278**, 127547 (2024).
45. Zhong, R. et al. Anti-aging mechanism and effect of treatment with raw and wine-steamed Polygonatum sibiricum on D-galactose-induced aging in mice by inhibiting oxidative stress and modulating gut microbiota. *Front. Pharmacol.* **15**, 1335786 (2024).
46. Kim, K. A., Jeong, J. J., Yoo, S. Y. & Kim, D. H. Gut microbiota lipopolysaccharide accelerates inflamm-aging in mice. *BMC Microbiol.* **16**, 9 (2016).
47. Cheng, L. H. et al. Lactobacillus paracasei PS23 improves cognitive deficits via modulating the hippocampal gene expression and the gut microbiota in D-galactose-induced aging mice. *Food Funct.* **13**, 5240–5251 (2022).
48. Coradduzza, D. et al. Age-related cognitive decline, focus on microbiome: a systematic review and meta-analysis. *Int. J. Mol. Sci.* **24**, 13680 (2023).
49. Liang, Z. et al. The potential of Klebsiella and Escherichia-Shigella and amino acids metabolism to monitor patients with postmenopausal osteoporosis in northwest China. *BMC Microbiol.* **23**, 199 (2023).
50. Atzeni, A. et al. Gut microbiota profile and changes in body weight in elderly subjects with overweight/obesity and metabolic syndrome. *Microorganisms* **9**, 346 (2021).
51. Markowiak-Kopec, P. & Slizewska, K. The effect of probiotics on the production of short-chain fatty acids by human intestinal microbiome. *Nutrients* **12**, 1107 (2020).
52. Abusleme, L. et al. The subgingival microbiome in health and periodontitis and its relationship with community biomass and inflammation. *ISME J.* **7**, 1016–1025 (2013).
53. Baek, K., Ji, S. & Choi, Y. Complex intratissue microbiota forms biofilms in periodontal lesions. *J. Dent. Res.* **97**, 192–200 (2018).
54. Turnbaugh, P. J. et al. The human microbiome project. *Nature* **449**, 804–810 (2007).
55. Yuan, Y., Yang, J., Zhuge, A., Li, L. & Ni, S. Gut microbiota modulates osteoclast glutathione synthesis and mitochondrial biogenesis in mice subjected to ovariectomy. *Cell Prolif.* **55**, e13194 (2022).
56. Mariat, D. et al. The Firmicutes/Bacteroidetes ratio of the human microbiota changes with age. *BMC Microbiol.* **9**, 123 (2009).
57. Sun, W. et al. Lonicera japonica polysaccharides alleviate D-galactose-induced oxidative stress and restore gut microbiota in ICR mice. *Int. J. Biol. Macromol.* **245**, 125517 (2023).
58. Morrison, D. J. & Preston, T. Formation of short chain fatty acids by the gut microbiota and their impact on human metabolism. *Gut Microbes* **7**, 189–200 (2016).
59. Santos, A. F. P., Cervantes, L. C. C., Panahipour, L., Souza, F. A. & Gruber, R. Proof-of-principle study suggesting potential anti-inflammatory activity of butyrate and propionate in periodontal cells. *Int. J. Mol. Sci.* **23**, 11006 (2022).
60. Wu, L. et al. Butyrate inhibits dendritic cell activation and alleviates periodontitis. *J. Dent. Res.* **102**, 1326–1336 (2023).
61. Yan, H. et al. Comparison of the gut microbiota in different age groups in China. *Front. Cell Infect. Microbiol.* **12**, 877914 (2022).
62. Sharma, R. & Diwan, B. Lipids and the hallmarks of ageing: From pathology to interventions. *Mech Ageing Dev.* **215**, 111858 (2023).
63. Romero-Marquez, J. M. et al. Molecular interactions between dietary lipids and bone tissue during aging. *Int. J. Mol. Sci.* **22,** 6473 (2021).
64. Nam, M. et al. Metabolic alterations in the bone tissues of aged osteoporotic mice. *Sci. Rep.* **8**, 8127 (2018).
65. Shao, L., Luo, S. & Zhao, Z. Lipid metabolites are associated with the risk of osteoporotic fractures. *Sci. Rep.* **14**, 19245 (2024).
66. Lee, C. T. et al. Subgingival microbiome and specialized pro-resolving lipid mediator pathway profiles are correlated in periodontal inflammation. *Front Immunol* **12**, 691216 (2021).
67. Sun, J. & Guo, G. Association between atherogenic index of plasma and periodontitis among U.S. adults. *BMC Oral Health* **23**, 166 (2023).
68. Stanisic, D. et al. Gut microbiota and the periodontal disease: role of hyperhomocysteinemia. *Can. J. Physiol. Pharmacol.* **99**, 9–17 (2021).
69. Botelho, J., Machado, V., Leira, Y., Proenca, L. & Mendes, J. J. Periodontal inflamed surface area mediates the link between homocysteine and blood pressure. *Biomolecules* **11**, 875 (2021).
70. Song, F. et al. Histamine deficiency deteriorates LPS-induced periodontal diseases in a murine model via NLRP3/Caspase-1 pathway. *Int Immunopharmacol* **115**, 109630 (2023).
71. Blancas-Luciano, B. E., Zamora-Chimal, J., da Silva-de Rosenzweig, P. G., Ramos-Mares, M. & Fernandez-Presas, A. M. Macrophages immunomodulation induced by Porphyromonas gingivalis and oral antimicrobial peptides. *Odontology* **111**, 778–792 (2023).
72. Yueyue Zhou, W. S., Wang, C., Changkao, Mu. & Li, R. Integrated metabolomics and transcriptomics reveal the anti-aging effect of melanin from Sepiella maindroni ink (MSMI) on D-galactose-induced aging mice. *Aging (Albany NY)* **13**, 11889–11906 (2021).
73. Zhou, Y. Y. et al. Gene transcriptional and metabolic profile changes in mimetic aging mice induced by d-galactose. *PLoS ONE* **10**, e0132088 (2015).
74. Tang, C. M. et al. Multi-omics reveals aging-related pathway in natural aging mouse liver. *Heliyon* **9**, e21011 (2023).
75. Houtkooper, R. H. et al. The metabolic footprint of aging in mice. *Sci. Rep.* **1**, 134 (2011).

Acknowledgements

We thank Zhongjia Tian, Hao Li for assistance with animal experiments and Professor Jianguo Liu for his support during the initial stage of this research.

Author contributions

F.L. analyzed the data and wrote this manuscript. Y.Y. conducted the animal experiments and collected the data. Y.H. and L. L. participated in the data and sample collection. Q.W. and B.C. reviewed the manuscript. H.H. designed the experimental study and reviewed the manuscript.

Funding
This study was supported by grants from the New Academic Talents Project of Zunyi Medical University (QKHPTRC [2018]5772–010), the Science and Technology Program of Guizhou Province (QKHJC-ZK [2022]-591), Young scientific and technological talents growth project of Guizhou Provincial Department of Education (NO: Qian Jiao He KY[2022]276).

Declarations

Competing interests
The authors declare no competing interests.

Additional information
Supplementary Information The online version contains supplementary material available at https://doi.org/10.1038/s41598-024-75941-w.

Correspondence and requests for materials should be addressed to H.H.